

# Beach-Profile Evolution under Spilling and Plunging Breakers

Ping Wang<sup>1</sup>; Bruce A. Ebersole<sup>2</sup>; and Ernest R. Smith<sup>3</sup>

**Abstract:** Beach-profile evolution, along with measurements of waves, currents, and sediment concentration, under spilling and plunging breakers of similar height were studied in the three-dimensional Large-Scale Sediment Transport Facility at the U.S. Army Engineer Research and Development Center. Unidirectional irregular waves were generated over a fine-sand beach. Beach-profile shape reached equilibrium after 1,330 and 280 min of spilling and plunging wave actions, respectively. Near the main breaker line, the profile evolved differently under plunging and spilling breakers. Across most of the midsurf zone dominated by surf bores, the equilibrium profile shapes were similar. Uniform energy dissipation per unit volume at equilibrium, as assumed in the Dean 1977 model and often used in cross-shore sediment-transport modeling, was measured for both cases across most of the surf zone except at the main breaker line, where a much greater rate of dissipation occurred. The bar/trough formation and maintenance were closely related to the local patterns of sediment suspension and bed scour at the plunging point.

**DOI:** 10.1061/(ASCE)0733-950X(2003)129:1(41)

**CE Database keywords:** Profiles; Sediment transport; Coastal morphology; Breaking waves.

## Introduction

The equilibrium concept is often embedded in modeling of beach-profile evolution. A commonly used assumption is that cross-shore sediment transport rate and therefore profile evolution depend on the deviation from an equilibrium state (e.g., Kriebel and Dean 1985; Kraus and Larson 1988). One of the most commonly used beach-profile models, which was developed by Dean (1977), is

$$h = Ax^{2/3} \quad (1)$$

where  $h$  = still-water depth,  $x$  = distance from the shoreline, and  $A$  = dimensional parameter determined by sediment grain size.

Various mechanisms have been suggested to explain beach-profile equilibrium in the surf zone. Two of the mechanisms that lead to Eq. (1) are examined here. The beach profile adjusts so that (1) the rate of wave-energy dissipation per unit water volume is uniform (Dean 1977), and (2) a nonlocal balance between on-shore sediment transport and offshore transport is reached (Larson et al. 1999).

Realizing that the forcing mechanisms landward and seaward of the breaker line are significantly different, Inman et al. (1993) and Larson et al. (1999) divided a beach profile into two independent portions separated at the breaker point. Power functions were used to model each section of the profile. The two-segment models are still monotonic and cannot reproduce the landward slope of the bar or bar crest. Wang and Davis (1998) added a third segment to represent the landward slope of the bar. The three-segment model improved the representation of barred profiles as indicated by a case study along the west-central Florida coast.

Bars/troughs are common dynamic nearshore features. Two general mechanisms have been developed to explain the formations of bars and troughs. One mechanism involves a convergence (at the bar) between offshore-direct sand transport carried by the undertow and an onshore transport due to wave asymmetry (Thornton et al. 1996). A second mechanism involves current patterns under standing or partially standing infragravity waves (Carter et al. 1973). Detailed patterns/gradients of sediment suspension at the breaker line and equilibrium of bar/trough features were not examined in these models.

In this study, beach-profile evolution was examined at the Large-Scale Sediment Transport Facility (LSTF). The objectives were to (1) investigate the beach-profile evolution under spilling and plunging breakers; (2) examine mechanisms that produce shoreface equilibrium; and (3) examine the equilibrium of bar/trough features.

## Methodology

The capabilities of the LSTF and procedures of establishing long-shore uniformity are discussed in Hamilton and Ebersole (2001). The beach is composed of approximately 150 m<sup>3</sup> of very well-sorted fine quartz sand with a median grain size of 0.15 mm. The sand beach was approximately 25 cm thick over a planar concrete

<sup>1</sup>Assistant Professor, Dept. of Geology, Univ. of South Florida, 4202 E. Fowler Ave., Tampa, FL 33620. E-mail: pwang@chumal.cas.usf.edu

<sup>2</sup>Research Engineer, U.S. Army Engineer Research and Development Center, Coastal and Hydraulics Laboratory, 3909 Halls Ferry Road, Vicksburg, MS 39180.

<sup>3</sup>Research Engineer, U.S. Army Engineer Research and Development Center, Coastal and Hydraulics Laboratory, 3909 Halls Ferry Road, Vicksburg, MS 39180.

Note. Discussion open until June 1, 2003. Separate discussions must be submitted for individual papers. To extend the closing date by one month, a written request must be filed with the ASCE Managing Editor. The manuscript for this technical note was submitted for review and possible publication on September 4, 2001; approved on July 10, 2002. This technical note is part of the *Journal of Waterway, Port, Coastal, and Ocean Engineering*, Vol. 129, No. 1, January 1, 2003. ©ASCE, ISSN 0733-950X/2003/1-41-46/\$18.00.

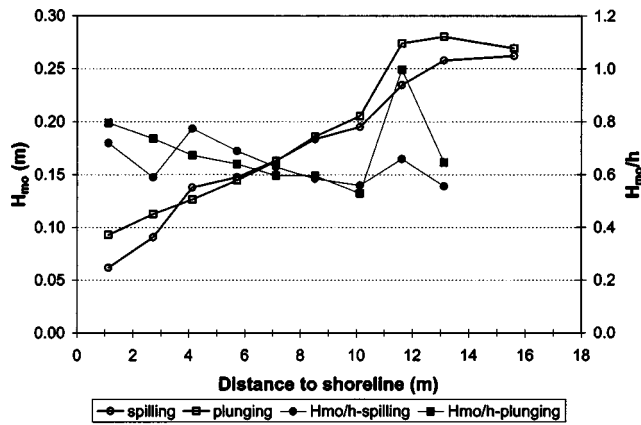


**Fig. 1.** Cross-shore distribution of significant wave height and the breaker index ( $H_{mo}/h$ ), measured at equilibrium conditions

base and extended 27 m alongshore and 18 m cross shore, of which 15 m were below still-water level and 3 m were above. The experimental procedures are discussed in Wang et al. (2002).

The spilling- and plunging-breaker cases lasted 1,990 and 630 min, respectively. The spilling-breaker experiment was conducted in eighteen 15–200 min segments, and the plunging case in thirteen 40–100 min segments. The LSTF hosts a suite of sensors measuring wave, current, and sediment concentration (Wang et al. 2002). All the sensors are mounted on a steel bridge that spans across the test beach. This bridge can be programed to move precisely along shore, allowing measurements to be made along transects at various longshore positions.

The beach profile was surveyed at the end of each wave-run segment using a bottom-tracking profiler that moved along the instrument bridge. The profiles were spaced at 1 m along shore and sampled at 0.5 cm cross shore. The vertical accuracy of the profiler was within 1.5 mm. The longshore gradients in longshore transport were negligible across the middle section of the test beach, and the longshore currents, mostly less than 20 cm/s, should not contribute significantly to sediment suspension (Wang et al. 2002). Therefore, beach-profile change should be mostly caused by gradients in cross-shore sediment transport. The following discussion is focused on the middle 15 m of the beach, where influences of lateral boundaries were minimal.

## Wave Conditions

The TMA spectrum with a spectral width parameter of 3.3 defined the incident wave (Wang et al. 2002). The main breaker line was located at 13.1 (second point from offshore) and 11.6 m (third point from offshore) from the shoreline for the spilling and plunging cases, respectively (Fig. 1). The main breaker line was determined to be at the location landward of which a significantly accelerated rate of wave-height decay was measured. This criterion was based on the comprehension that a substantial wave-energy loss, and therefore, wave-height decrease, should follow major wave breaking.

Similar breaker heights of 0.26 and 0.27 m were measured for the spilling and plunging cases, respectively. The accuracy of the capacitance wave gauges was  $\pm 2$  mm (Wang et al. 2002). The ratio of significant wave height ( $H_{mo}$ ) to still-water depth ( $h$ ), the breaker index, ranged mostly from 0.6 to 0.8 (Fig. 1). A large value, nearly 1.0, was measured at the plunging breaker line,

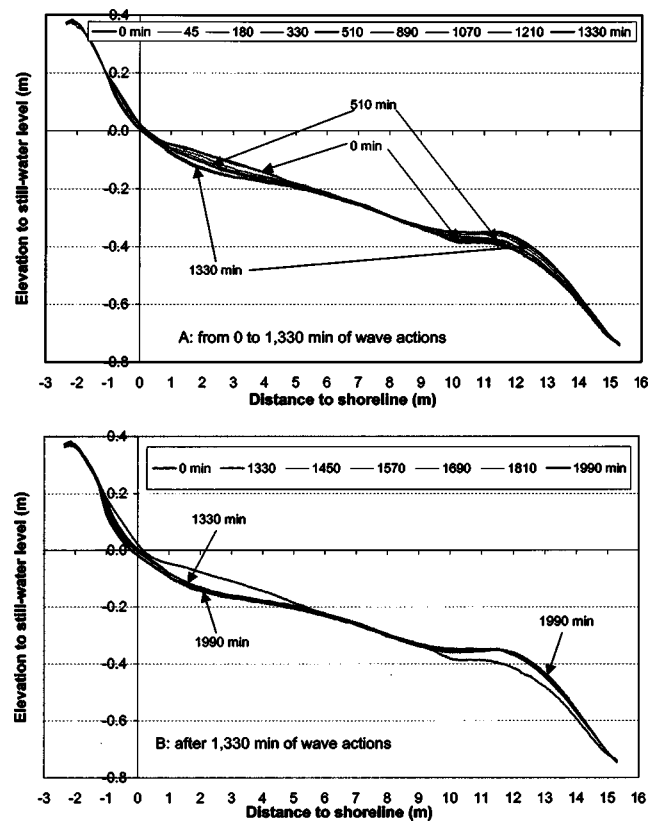


**Fig. 2.** Beach-profile evolution, spilling case

followed by a sharp decline to slightly less than 0.6. A trend of landward increase of the  $H_{mo}/h$  ratio, from slightly below 0.6 to nearly 0.8, was measured across most of the surf zone for both the spilling and plunging cases. Similar values of  $H_{mo}$  and  $H_{mo}/h$  were measured in the surf-bore dominated midsurf zone for both cases, while conditions near the main breaker line and the shoreline were different (Fig. 1).

## Results and Discussion

### Beach-Profile Evolution

The beach was initially constructed based on the Dean (1977) model [Eq. (1)]. The average of the middle 15 profiles serves as a representative profile. The spilling-breaker experiment was conducted with the constructed beach as the initial condition. Most of the beach-profile change occurred during the first 1,330 min of wave action [Fig. 2(A)]. In Fig. 2 and the following figures, the shoreline in the horizontal axis was defined as that of the initially constructed beach, which was 3.0 m from the basin wall. During the first 1,330 min, the inner surf zone from 1 to 5 m experienced erosion. The outer surf zone from 5 to 9 m remained stable. Sand accumulation occurred in the vicinity of the breaker line from 9 to 14 m, the source of which was apparently the erosion in the inner surf zone. In Fig. 2(A), profiles at 0, 510, and 1,330 min were highlighted; profiles at other times (thin lines) followed the same trend. After 1,330 min, the rate of profile change was small; profiles at 0, 1,330, and 1,990 min were highlighted [Fig. 2(B)]. In order to induce characteristic spilling breakers, waves with a steepness of 0.08 were generated. These steep waves are responsible for the persistent erosion at the shoreline (Fig. 2).

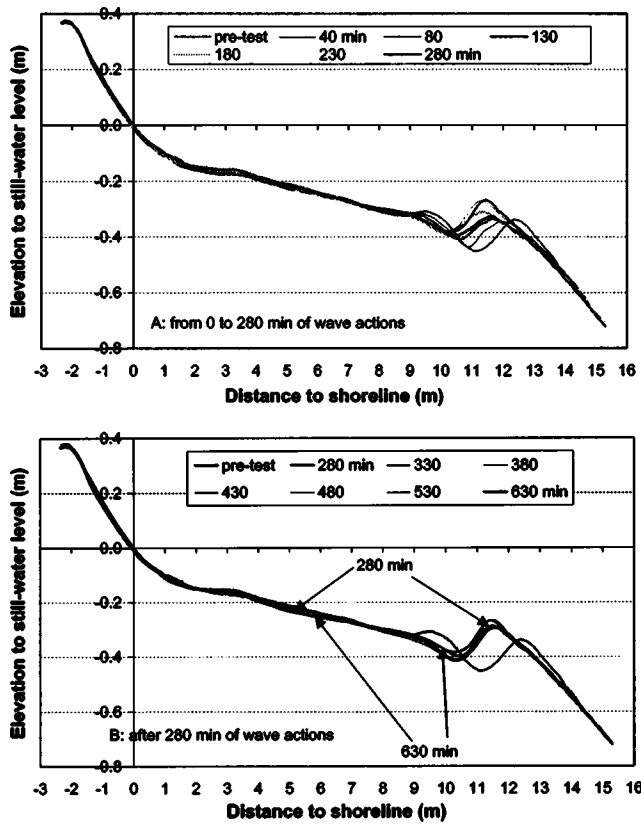


Fig. 3. Beach-profile evolution, plunging case

A higher wave of  $H_{mo} = 0.45$  m was run before the plunging case, resulting in the development of a substantial offshore bar just outside the surf zone. In response to the reduced wave height, a landward migration of the offshore bar occurred [Fig. 3(A)]. This bar migration resulted in substantial elevation gain in the previous trough and elevation loss at the previous bar crest and its seaward slope. The secondary bar that had developed just landward of the original trough between 9 and 10 m was eroded, and the sand was apparently transported a short distance seaward and contributed to the building of the new bar. The new bar crest was located at the position of the previous trough, and the previous secondary bar became the landward slope of the new trough. These changes occurred in a narrow zone between 9 and 14 m near the main plunging breaker line during a 280 min wave action. The volume eroded equaled roughly to the volume gained at the new bar. Little change occurred at the seaward limit of the profiles, near the shoreline, and across most of the midsurf zone.

Magnitudes of profile change between 280 and 630 min were much smaller than those before 280 min, indicating that the beach has approached equilibrium [Fig. 3(B)]. The landward migration of the bar was replaced by irregular and minor variations. In Fig. 3(B), the profiles at 280 and 630 min were highlighted; profiles at other times (thin lines) did not follow the same trend. Persistent shoreline erosion measured during the spilling case (Fig. 2) was not apparent during the plunging case (Fig. 3). The steep offshore toe may influence wave shoaling and refraction. However, since measured in situ breaking wave conditions are used here, this influence should already be incorporated.

### State of Equilibrium

The beach reached equilibrium, or stable shape, after 1,330 and 280 min of spilling and plunging wave action, respectively. Here,

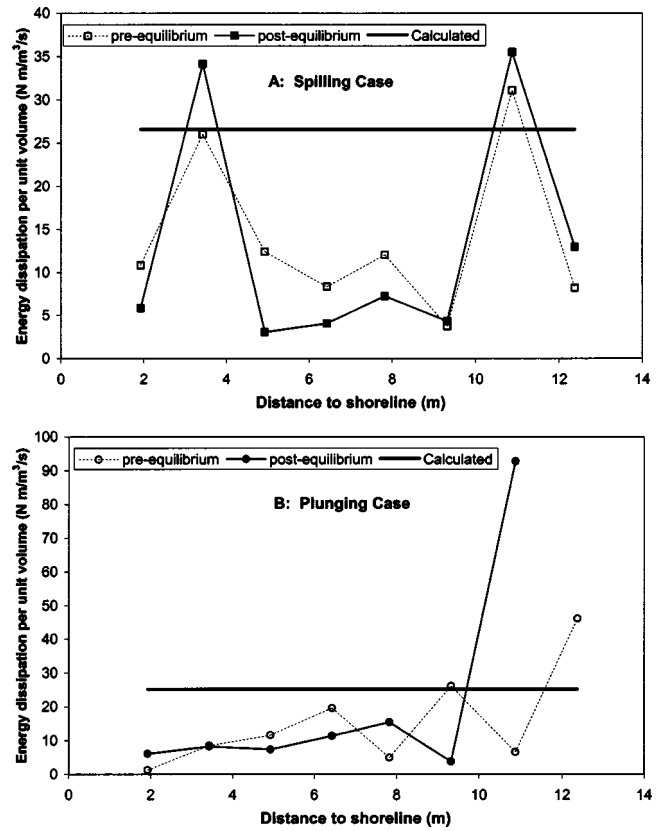


Fig. 4. Cross-shore distribution of  $D(x)$ , at the beginning of the experiment and at equilibrium

the equilibrium profiles for the spilling and plunging cases are represented by the time averages between 1,330 and 1,990 min and 280 and 630 min, respectively.

### Uniform Energy Dissipation per Unit Volume

Dean (1977) related the equilibrium profile [Eq. (1)] to uniform wave-energy dissipation per unit volume. The wave-energy dissipation per unit volume,  $D(x)$ , is determined as

$$D(x) = \frac{1}{h} \frac{\partial(EC_g)}{\partial x} = \frac{1}{h} \frac{\partial \left( \frac{1}{8} \rho g H_{rms}^2 \sqrt{gh} \right)}{\partial x} \quad (2)$$

where  $H_{rms}$  = root-mean-square wave height, and equals  $0.71 H_{mo}$  assuming a Rayleigh distribution of wave height. The  $H_{rms} = 0.71 H_{mo}$  values are used here instead of the values obtained through zero-crossing analyses because this assumption is often used in modeling efforts.  $D(x)$  was calculated from the measurements at two adjacent wave gauges and represented at the midpoint. The wave gauges were spaced at 1.5 m apart. The energy-dissipation rate obtained from the two closely spaced gauges should be reliable. The energy-dissipation patterns were calculated at the beginning and end of each wave case. The purpose was to examine the adjustment of wave-energy dissipation as the profile approached equilibrium.

For the spilling case, the overall energy-dissipation patterns before (0–45 min) and after the equilibrium (average between 1,330 and 1,990 min) were similar [Fig. 4(A)]. A steep gradient in  $D(x)$  occurred at the main breaker line. Another peak occurred at approximately 3.4 m, the reason for which was not clear. Except for these two locations,  $D(x)$  was fairly uniform after the equi-

librium. Prior to equilibrium, greater  $D(x)$  occurred at most of the locations except at the two peaks. Modest improvement in uniformity across the surf zone occurred after the beach reached equilibrium.

For the plunging case,  $D(x)$  patterns were significantly different before (0–40 min) and after (average between 280 and 630 min) equilibrium [Fig. 4(B)]. Before equilibrium,  $D(x)$  varied considerably across the surf zone, with an overall landward-decreasing trend. At equilibrium, the  $D(x)$  value was nearly one order of magnitude greater at the main breaker line than those at the rest of the surf zone, where  $D(x)$  was reasonably uniform.

Based on the analyses of Dean (1977), equilibrium energy dissipation per unit volume,  $D_*$ , can be calculated as

$$D_* = \frac{5}{24} A^{3/2} \rho g \sqrt{g} \gamma^2 \quad (3)$$

where  $\gamma$  = breaker index. The  $\gamma$  value, determined here as  $H_{m0}/h$  ranged from 0.6 to nearly 1, and varied across the surf zone (Fig. 1). The average  $\gamma$  value was 0.66 for the spilling case and 0.64 for the plunging case. Because  $H_{rms}$  was used to calculate the wave energy [Eq. (2)], the breaker index corresponding to  $H_{rms}$  ( $\gamma_{rms} = H_{rms}/h$ ) was 0.47 for the spilling case and 0.45 for the plunging case.

The calculated  $D_*$  using  $\gamma_{rms}$  [Eq. (3)] is on average 480% (excluding the near-shore peak and the breaker-line peak) greater than the measured  $D(x)$  for the spilling case and 250% (excluding the breaker-line peak) greater for the plunging case (Fig. 4). At the breaker line,  $D_*$  was 30% less than the measured  $D(x)$  for the spilling case and 270% less for the plunging case.

The derivation of Dean (1977) was conducted under the assumption of spilling breakers. The similar dissipation patterns before and after equilibrium for the spilling case were probably because the initial beach was close to equilibrium. The significantly greater  $D(x)$  at the plunging breaker line corresponds with the local deviation from the power function. The region having relatively uniform energy dissipation coincided with the portion of the surf zone that is dominated by surf bores.

### Nonlocal Balance of Onshore and Offshore Sediment Transport

Larson et al. (1999) derived the equilibrium profile (Eq. 1) by balancing the gradient of near-bottom undertow-driven offshore transport with a vertical transport due to net sedimentation (or suspension). Cross-shore sediment flux,  $F_{cs}(x, z, t)$ , is calculated as

$$F_{cs}(x, z, t) = u(x, z, t) \times c(x, z, t) \quad (4)$$

where  $u$  = cross-shore current, and  $c$  = sediment concentration. To simplify the complex temporal variations of the surf-zone sediment motion, current velocity and sediment concentration were often partitioned as (e.g., Osborne and Greenwood 1992; Thornton et al. 1996)

$$u = \bar{u} + \tilde{u}_{low} + \tilde{u}_{high} \quad (5)$$

$$c = \bar{c} + \tilde{c}_{low} + \tilde{c}_{high} \quad (6)$$

where  $\bar{u}$  and  $\bar{c}$  = time-averaged velocity and sediment concentration, respectively.  $\tilde{u}$  and  $\tilde{c}$  are oscillatory components of velocity and concentration. The subscripts *high* and *low* indicate high- and low-frequency components. The time-averaged sediment flux at location  $(x, z)$  is determined as

$$\overline{F_{cs}} = \overline{uc} = \bar{u} \bar{c} + \overline{\tilde{u}_{low} \tilde{c}_{low}} + \overline{\tilde{u}_{high} \tilde{c}_{high}} \quad (7)$$

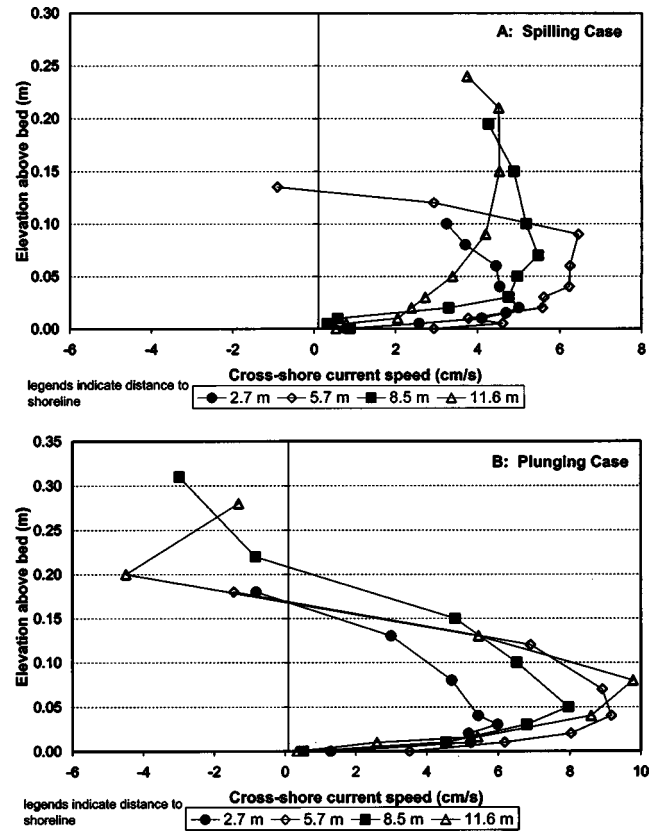


Fig. 5. Profiles of undertow through the water column

Osborne and Greenwood (1992) found that in different parts of the surf zone, the direction and magnitude of cross-shore transport were dominated by different terms. In general, offshore-directed transport is dominated by the undertow while the asymmetrical oscillatory motions dominated onshore-directed transport. The transport by oscillatory motions was not considered in Larson et al. (1999) analysis; offshore-directed transport was assumed to be driven by undertow.

Vertical profiles of cross-shore current were measured at the ten cross-shore locations after the beaches reached equilibrium (Fig. 5). Undertow was measured through most of the water column below the wave trough. Time-averaged sediment-concentration profiles demonstrated rapidly upward-decreasing trends over nearly four orders of magnitude. One exception occurred at the main plunging breaker line, where the variation spanned only one order of magnitude (Wang et al. 2002). If oscillatory transport is neglected, the time-averaged cross-shore-flux profile obtained from the product of time-averaged profiles of current and sediment concentration is dominantly offshore directed and exhibits a steep upward-decreasing trend (Fig. 6).

Larson et al. (1999) balanced the gradient of offshore transport by undertow with a net vertical sedimentation (or suspension) as

$$\frac{dF_{offshore}}{dx} = \frac{d(q_{undertow}c_0)}{dx} = \mu w c_0 \quad (8)$$

where  $F_{offshore}$  = depth-integrated offshore flux,  $q_{undertow}$  = discharge of undertow,  $c_0$  = characteristic sediment concentration,  $\mu$  = empirical coefficient, and  $w$  = sediment fall speed. A nonlocal balance implies, as illustrated in the Fig. 1 of Larson et al. (1999), that an offshore-increasing undertow transport can be nonlocally balanced by sedimentation from net onshore trans-

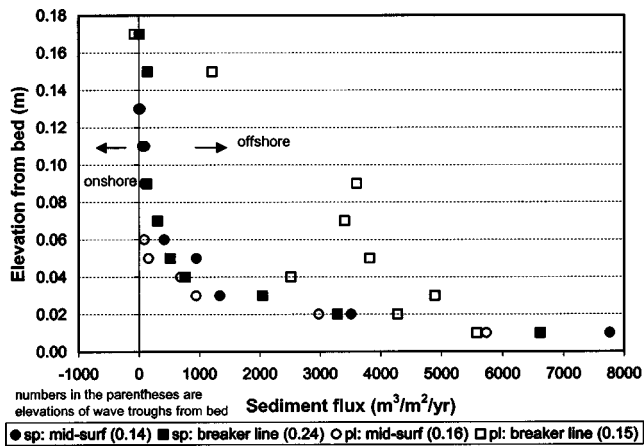


**Fig. 6.** Product of time-averaged profiles of sediment concentration and cross-shore current

port near the water surface. An offshore-decreasing undertow transport can be balanced by sediment suspension and horizontal dispersion.

From the trends shown in Fig. 6, the circulation schematized in the Fig. 1 of Larson et al. (1999) cannot be achieved without considering the oscillatory terms. Fig. 7 shows depth-integrated offshore transport by undertow over the equilibrium beach. A peak and a trough occurred at around 6 and 8 m, respectively, for the spilling case. Nearly no bed-level change was measured at both locations (Fig. 2). For the plunging case, a high transport peak occurred just landward of the bar crest. This steep gradient had to be balanced by onshore processes because bed-level change was negligible at equilibrium. Fig. 7 also indicates that gradients in undertow transport alone are not directly linked to profile evolution. The cross-shore patterns of undertow speed did not appear to correspond significantly to beach-profile evolution for both cases, when the time-series patterns were compared.

### Observations of Bar/Trough Formation and Equilibrium under Plunging Breakers

Formation of the bar/trough seemed to be related to local patterns of sediment motion under the plunging breakers. The main plunging point coincided with the trough location. A large portion of the suspended sediment agitated by the downward jet tended to

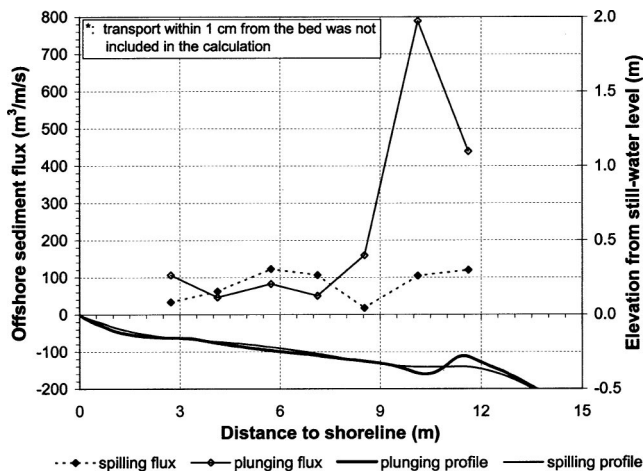


**Fig. 7.** Offshore sediment transport by undertow

move offshore toward the bar crest, carried by the undertow. A small portion was moved onshore, leading to the formation of a secondary bar just landward of the trough. This secondary bar was apparent during the higher wave run before the plunging case [Fig. 3(A)], and became less distinctive when the wave height was reduced [Fig. 3(B)]. Ting and Kirby (1995) found that turbulent energy generated by plunging breakers tends to be transported onshore, which may explain the onshore dispersion of sediment suspended at the plunging point and development of the secondary bar.

Onshore sand transport, in the form of a thin layer sliding across the bar crest and down the steep landward slope ( $\sim 1:7$ ), was observed as the wave crests passed over the bar just before breaking. The dynamic equilibrium of the bar/trough system was maintained by the balance between the onshore transport attributed to gravity and the onshore component of the orbital velocity at the landward bar slope and the offshore transport caused by a combination of active sediment suspension by the plunging jet and the undertow. These localized sediment motions need to be considered in bar/trough models.

### Summary

The beach profiles reached equilibrium after approximately 1,330 and 280 min of the spilling and plunging wave actions, respectively. The difference in time to reach equilibrium was influenced by differences between the starting and ending profile shapes, and transport intensity. Different rates and patterns of profile evolution were measured near the main spilling and plunging breaker lines. Across most of the midsurf zone, the shapes of the equilibrium profiles were similar.

Uniform energy dissipation per unit volume at equilibrium, as suggested by Dean (1977), was measured across most of the surf zone except near the main breaker line, where a much faster dissipation rate occurred. The measured equilibrium dissipation was considerably smaller than the predictions from the Dean 1977 model. The product of the time-averaged profiles of cross-shore current and sediment concentration yielded a net offshore-directed sediment transport. The near-surface onshore transport necessary for the non-local-balance equilibrium as suggested by Larson et al. (1999) could not be identified from the time-averaged current and sediment concentration.

A pronounced bar developed during the plunging case. Development/maintenance of the bar/trough system is related to local patterns of sediment motion near the plunging breaker line. Formation of the trough is related to the scour of the downward jet at the plunge point, and the offshore dispersion of the suspended sediment contributed to the bar building. The equilibrium bar/trough system seemed to be maintained by a balance between onshore transport attributed to gravity and the onshore component of orbital velocity at the landward bar slope and the offshore transport caused by the dramatic sediment suspension at the trough induced by the plunging jet and the undertow.

### Acknowledgments

The writers thank Carl Miller and Reggie Beach for providing the FOBS sensors and Dr. N. C. Kraus for an earlier review. One of the writers (P.W.) is partially funded by the Louisiana Sea Grant College Program. Permission to publish this paper was granted by the Headquarters, U.S. Army Corps of Engineers.

## References

- Carter, T. G., Liu, P. L. F., and Mei, C. C. (1973). "Mass transport by waves and offshore sand bedforms." *J. Waterw., Port, Coastal Ocean Div., Am. Soc. Civ. Eng.*, 99(2), 165–184.
- Dean, R. G. (1977). "Equilibrium beach profiles: U.S. Atlantic and Gulf coasts." *Ocean Eng. Rep. No. 12*, Dept. of Civil Eng., Univ. of Delaware, Newark, Del.
- Hamilton, D. G., and Ebersole, B. A. (2001). "Establishing uniform long-shore currents in a large-scale laboratory facility." *Coastal Eng.*, 42, 199–218.
- Inman, D. L., Elwany, M. H. S., and Jenkins, S. A. (1993). "Shorerise and bar-berm profiles on ocean beaches." *J. Geophys. Res.*, 98(C10), 18, 181–188, and 199.
- Kraus, N. C., and Larson, M. (1988). "Prediction of initial profile adjustment of nourished beaches to wave action." *Proc., 1988 National Conf. on Beach Preservation Technology*, pp. 125–137.
- Kriebel, D. L., and Dean, R. G. (1985). "Numerical simulation of time-dependent beach and dune erosion." *Coastal Eng.*, 9, 221–245.
- Larson, M., Kraus, N. C., and Wise, R. A. (1999). "Equilibrium beach profiles under breaking and nonbreaking waves." *Coastal Eng.*, 36, 59–85.
- Osborne, P. D., and Greenwood, B. G. (1992). "Frequency-dependent cross-shore suspended sediment transport. 2: A barred shoreface." *Mar. Geol.*, 106, 25–51.
- Thornton, E. B., Humiston, R. T., and Birkemeier, W. (1996). "Bar/trough generation on a natural beach." *J. Geophys. Res.*, 101, 12, 97–12, and 110.
- Ting, F. C. K., and Kirby, J. T. (1995). "Dynamics of surf-zone turbulence in a strong plunging breaker." *Coastal Eng.*, 24, 177–204.
- Wang, P., and Davis, R. A. (1998). "Beach profile model for a barred coast—Case study from Sand Key, west-central Florida." *J. Coastal Res.*, 14, 981–991.
- Wang, P., Smith, E. R., and Ebersole, B. A. (2002). "Large-scale laboratory measurements of longshore sediment transport under spilling and plunging breakers." *J. Coastal Res.*, 18, 118–135.